Scripta Materialia 179 (2020) 49–54

Contents lists available at ScienceDirect

Scripta Materialia

journal homepage: www.elsevier.com/locate/scriptamat

Activation and suppression of ⟨c + a⟩ dislocations in a textured Mg–3Al–1Zn alloy

Dexin Zhao[a], Xiaolong Ma[a,*], Sezer Picak[a,b], Ibrahim Karaman[a,b], Kelvin Xie[a,*]

[a] Department of Materials Science and Engineering, Texas A&M University, College Station, TX 77843, USA
[b] Department of Mechanical Engineering, Texas A&M University, College Station, TX 77843, USA

ARTICLE INFO

Article history:
Received 25 October 2019
Revised 10 November 2019
Accepted 26 November 2019
Available online 17 January 2020

Keywords:
<c + a> dislocation
Texture
Mg–3Al–1Zn
Correlative microscopy

ABSTRACT

In this work, we statistically studied the activation and suppression of ⟨c + a⟩ dislocations in a textured Mg–3Al–1Zn alloy after compression. Our results revealed that the activation and suppression of ⟨c + a⟩ dislocations in polycrystals are primarily governed by the overall texture, regardless of the crystallographic orientation of each grain. This observation is explained by the requirement of five independent slip systems, reduced anisotropy, and twin-induced strain localization. These direct observations of ⟨c + a⟩ dislocation activities offer a key insight into understanding the deformation mechanism of polycrystalline Mg alloys.

Magnesium (Mg) and its alloys have attracted extensive research interests as they are promising lightweight and high specific strength structural materials. However, pure Mg and most Mg alloys are brittle and difficult to form at room temperature [1–3]. The limited ductility and formability are attributed to the low mobility of pyramidal ⟨c + a⟩ dislocations, which usually accommodate *c-axis* compression [4–11]. Thus, the detailed understanding of ⟨c + a⟩ dislocation behavior could potentially guide the design of ductile and formable Mg alloys.

The activation of pyramidal slip has been well studied in Mg single crystals [4,12–17]. When compressed along the *c-axis*, ⟨c + a⟩ dislocations were observed to be the dominant deformation mechanism. Obara et al. [12] performed detailed two-beam condition analyses using transmission electron microscopy (TEM) and concluded that the Burgers vector of ⟨c + a⟩ dislocations is ⟨11–23⟩ [12]. Recent experimental studies [4,18] and molecular dynamics simulations [19] demonstrated that ⟨c + a⟩ dislocations can glide on both {10–11} pyramidal I and {11–22} pyramidal II planes. The critical resolved shear stress (CRSS) of ⟨c + a⟩ pyramidal slip measured ~40 MPa [12], which is much higher than that of basal slip (0.5 MPa, with the Burgers vector <11–20>) [5,20]. Due to this substantial anisotropy, if the *c-axis* is a few degrees off the loading direction in Mg single crystals, according to Schmid's law, basal ⟨a⟩ slip will be activated to accommodate the plastic deformation. As a result, ⟨c + a⟩ slip will be suppressed.

The ⟨c + a⟩ dislocation activities in polycrystalline Mg samples are more complex than in single crystals [21]. When compressing a hot-rolled Mg plate along the normal direction, although many grains have their *c-axis* aligned close to the loading direction, the activation of ⟨c + a⟩ dislocations could depend on two factors: 1) the orientation of the individual grain and 2) the global texture of the bulk material. For a grain whose *c*-axis is aligned away from the loading direction, the Schmid factor analysis predicts no or very few ⟨c + a⟩ dislocations in such grain, as the basal slip would be the dominant deformation mechanism. On the other hand, the deformation of such grain may also be constrained by the highly textured neighboring grains to satisfy strain compatibility, leading to profuse ⟨c + a⟩ dislocation activities. The scientific question we aim to answer is *which of the two aforementioned factors – the individual grain orientation or the global texture – is more dominant for ⟨c + a⟩ dislocation activation*. In this work, we selected a highly textured hot-rolled Mg–3Al–1Zn (AZ31) as the model material and developed a correlative microscopy technique to link the crystal orientation with the ⟨c + a⟩ dislocation microstructure to address the above question.

A hot-rolled AZ31 sheet was purchased from *MetalMart International Inc.* The bulk sample was annealed at 350 °C for 12 h with Ar flow to remove the stored dislocations. Rectangular compression specimens (4 mm × 4 mm × 8 mm) were electrical discharge machined (EDM) from the center of the hot-rolled plate. Quasi-static compression tests were conducted along the normal direction (ND) and 45° off-normal direction (refer to 45°) at a strain rate of 5×10^{-4} s^{-1}. The representative stress-strain curves were obtained from two specimens compressed to failure. All presented

* Corresponding authors.
E-mail addresses: xlma@tamu.edu (X. Ma), kelvin_xie@tamu.edu (K. Xie).

https://doi.org/10.1016/j.scriptamat.2019.11.057
1359-6462/

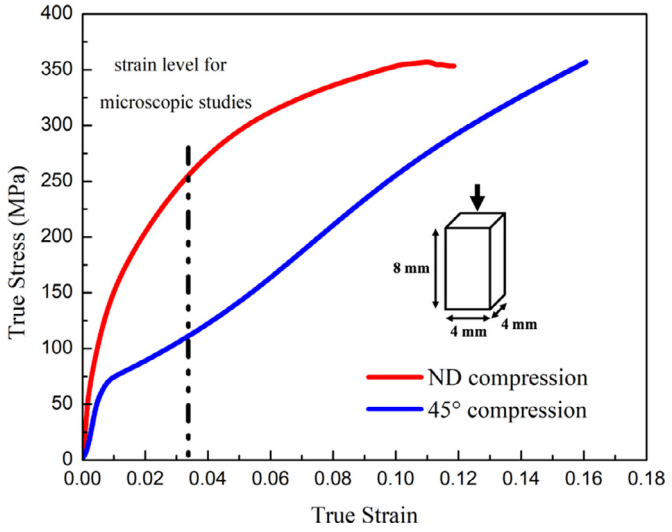

Fig. 1. Stress–strain curves of polycrystal hot-rolled Mg AZ31 alloy (after heat treatment) under compression along normal direction (ND compression, close to *c-axis*) and 45° off normal direction (45° compression).

Table 1
The *c-axis* off-angle and the corresponding existence of $\langle c + a \rangle$ dislocations based on TEM observations in 19 and 12 randomly selected grains from ND and 45° compression samples, respectively.

ND compression			45° compression		
Grain	*c-axis* off angle	$<c + a>$	Grain	*c-axis* off angle	$<c + a>$
1	2.16°	yes	1	4.33°	no
2	7.35°	yes	2	6.88°	no
3	9.03°	yes	3	10.1°	no
4	10.16°	yes	4	19.16°	no
5	11.25°	yes	5	20.51°	no
6	12°	yes	6	21.65°	no
7	13.83°	yes	7	27.32°	no
8	14.78°	yes	8	30.86°	no
9	15.77°	yes	9	35.67°	no
10	16.90°	yes	10	40.99°	no
11	18.37°	yes	11	41.19°	no
12	18.8°	yes	12	54.34°	no
13	19.04°	no			
14	19.17°	yes			
15	19.82°	yes			
16	22.49°	yes			
17	25.38°	yes			
18	25.71°	yes			
19	28.79°	yes			

microscopy studies were performed on the specimens compressed to ~2.6% plastic strain.

Correlative microscopy specimens were cut from the center region of the compression samples. To measure the off-angle between the *c-axis* of the grains of interest and the loading axis, non-circular TEM foils with one straight edge parallel to loading direction were fabricated. These discs were then twin-jet electropolished using a *Tenupol-5* polishing system with a solution of 15.9 g lithium chloride, 33.5 g magnesium perchlorate, 1500 ml methanol and 300 ml 2-butoxy-ethanol at −40 °C. Electron backscattered diffraction (EBSD) was carried out on TEM foils after ion mill at liquid nitrogen temperature using a *Tescan FERA* scanning electron microscope equipped with an EBSD detector from *Oxford Instrument*. Dislocations were imaged using the 2-beam bright-field (BF) and weak beam dark-field (WBDF) techniques on an *FEI Tecnai* TEM operating at 200 keV. To reveal the dislocation characters, we performed careful tilting experiments in TEM and used $\mathbf{g}\,\mathbf{b} = 0$ invisibility criteria to separately illuminate $\langle a \rangle$ and $\langle c \rangle$ components. The **g**-vectors we used to illuminate dislocations are $\mathbf{g} = [0002]$ (all *c*-component will be visible) and $\mathbf{g} = [01\text{–}10]$ (two-thirds of *a*-component will be visible). If a dislocation is visible under both $\mathbf{g} = [0002]$ and $\mathbf{g} = [01\text{–}10]$ conditions, it is of $\langle c + a \rangle$ type. We randomly selected 19 grains for ND compression samples and 12 grains for 45° compression samples to study the dislocation activities statistically, from which 5 and 6 representative grains were used to elucidate the general observations for each case, respectively.

The mechanical properties of the hot-rolled AZ31 in this study are consistent with what has been reported in the literature [22,23]. As shown in Fig. 1, the ND compression stress-strain curve does not show a sharp yielding transition. The yield strength, ultimate compressive strength and strain to failure were measured to be 107 ± 4 MPa, 296 ± 18 MPa, and 9.9% ± 0.8%, respectively. The 45° compression sample curve shows a clear yield transition. The yield strength, ultimate compressive strength, and strain to failure were measured to be 71 ± 1.4 MPa, 355 ± 2.5 MPa, and 16.5% ± 0.5%, respectively. The global EBSD inverse pole figure (IPF) of the as-hot-rolled sample confirmed the strong *c-axis* texture along the ND (Figs. 2(a)). The average grain size measured is approximately 10 μm. For the ND samples, the *c-axis* texture did not change significantly after compression (an example see Figs. 2(b)). This was expected, as dislocation-mediated plasticity is the predominant deformation mode. Very few {10–12} twins were noted but they are not a prominent microstructural feature. For 45° compression samples, high-density {10–12} extension twins (an example see Fig. 2(c)) were observed.

To uncover the detailed deformation mechanisms of individual grains in the samples, EBSD and TEM were performed on the same set of grains to correlate the crystal orientation with the dislocation activities. The off-angles between the *c-axis* of each grain and the loading direction were firstly identified by EBSD, and the dislocation activities in the corresponding grains were examined afterward. Fig. 3 shows the observation from the ND-compression sample. The compression direction is marked by the black arrows above each IPF map. The dark feature in the middle of each map is the perforated hole produced by electropolishing. Adjacent to the hole is the electron transparent area for both EBSD mapping and TEM imaging. In the EBSD maps, the grains of interest are in bright colors, with the rest being partly greyed out. We note that, despite the strong texture, there are a significant number of grains with their *c-axis* off the compression direction by larger angles (some even off by more than 20°). The orientations of the inspected grains are indicated by the crystal schematics in Fig. 3(a and b), which are listed in Table 1. Schmid factors of Pyramidal I, II $\langle c + a \rangle$, basal $\langle a \rangle$, and prismatic $\langle a \rangle$ dislocations for each grain are also summarized in Table S1. Thus, despite the overall strong texture, there exist many individual grains exhibiting non-negligible off-angles.

For the ND compression sample, we observed that $\langle c + a \rangle$ dislocations exist in 18 grains out of 19, regardless of the magnitude of off-angle. For example, profuse $\langle c + a \rangle$ dislocations were observed in Grain 1, where the off-angle is relatively small (2.16°). This observation is consistent with our expectation based on single-crystal studies [24] that $\langle c + a \rangle$ dislocations are required to accommodate near- *c-axis* compression. However, as shown in Fig. 3, numerous $\langle c + a \rangle$ dislocations were also observed in other grains with large off-angles. An example of Grain 19 whose off-angle is up to 28.79°. The $\langle c + a \rangle$ dislocations in this grain appear at least as rich as, if not more than, pure $\langle a \rangle$ dislocations. This is in stark contrast to the case in single crystal studies, where no or limited $\langle c + a \rangle$ dislocations should be observed when the off-angle is large [16]. The only grain that is free of $\langle c + a \rangle$ dislocations in the 19 observed grains is Grain 13 with off-angle 19.04° (Fig. 3(h)). The absence of $\langle c + a \rangle$

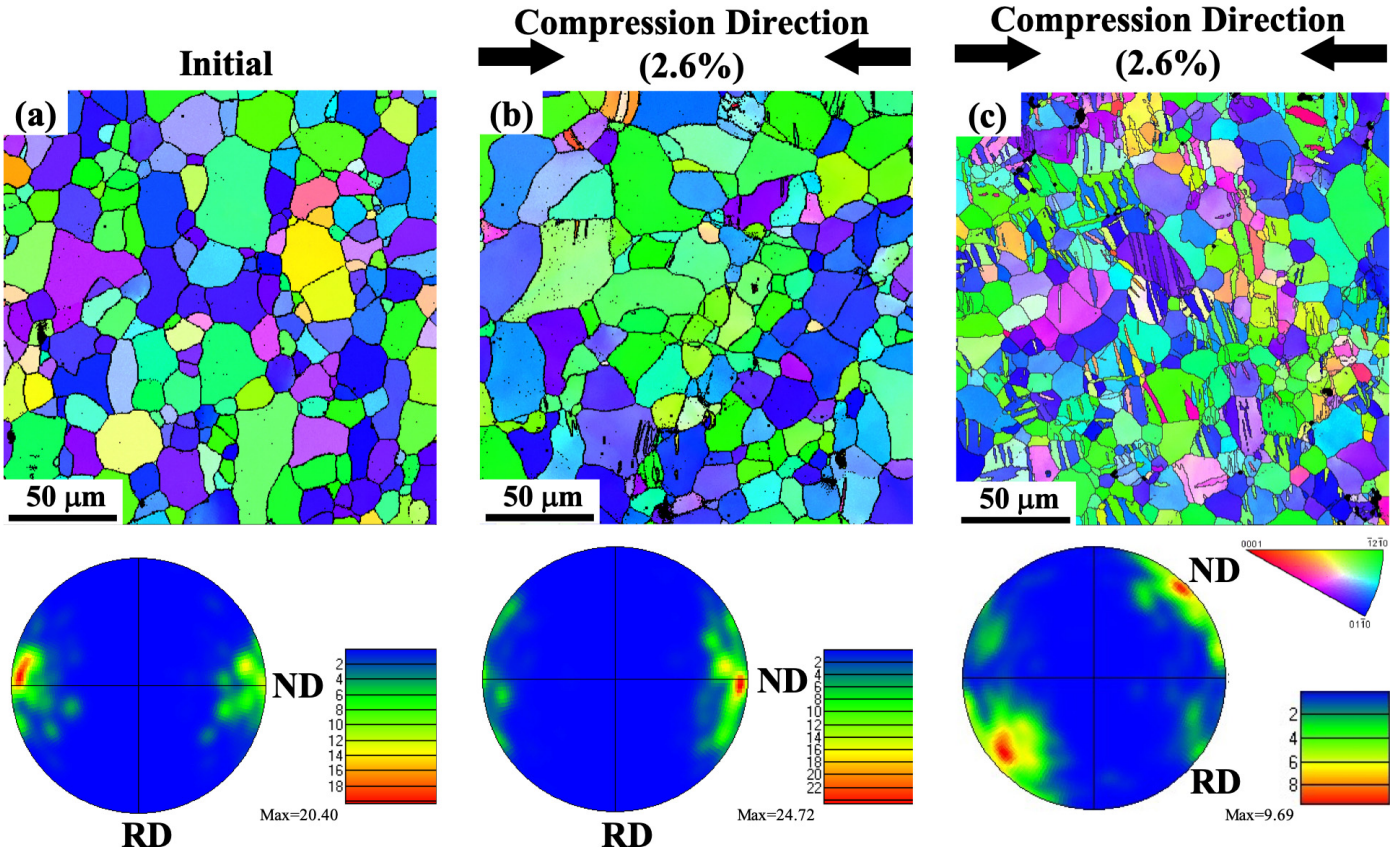

Fig. 2. EBSD IPF maps (out-of-plane crystal orientation) of AZ31 (a) initial, (b) compression along the normal direction (2.6% plastic strain) and (c) compression along 45° off normal direction (2.6% plastic strain), along with the corresponding (0001) pole figures and their highest mud values.

dislocation is likely a stochastic outlier. We further compared the $\langle c+a\rangle$ dislocations and noticed they share the same morphology and slip behavior. For example, many $\langle c+a\rangle$ dislocations appear to be basal-bound when imaged with $\mathbf{g}=[0002]$, regardless of the off-angles.

For the 45° compression sample, the same methodology was adopted to characterize the crystallographic orientation and dislocation activities using both EBSD (Fig. 4(a)) and TEM (Fig. 4(b–g)). In contrast to the ND compression sample, none of those grains shows apparent $\langle c+a\rangle$ dislocations (Table 1) and most dislocations observed only have $\langle a\rangle$ character. This is the case even for those grains with small off-angles (*c-axis* close to the loading direction), as shown in Figs. 3(b and c). Note, individual grains with similar orientations in the ND samples contain numerous $\langle c+a\rangle$ dislocations, whereas only $\langle a\rangle$ dislocations were observed in the 45° samples. We also noticed that the $\langle a\rangle$ dislocation morphology differs according to the off-angle value. For those with small off-angles, both basal and non-basal $\langle a\rangle$ dislocations are activated; for those with large off-angles (*c-axis* far away from the loading direction), basal $\langle a\rangle$ prevails.

The activation and suppression of $\langle c+a\rangle$ dislocations, supported by the statistics from both the ND and 45° samples, offer strong experimental evidence that texture plays a more dominant role than the orientation of individual grains in Mg. Even for grains with the off-angles presumably high or low enough to transit the governing dislocation mechanism, the global texture appears to inhibit such transition. We suggest that three factors contribute to this texture-governed dislocation activity.

First of all, unlike in single crystal, deformation in polycrystals requires five independent slip systems to accommodate the global strain according to von Mises condition [25]. In Mg, basal and prismatic only provide two each. Additional deformation mode, usually extension twinning or $\langle c+a\rangle$ pyramidal slip, has to come into play. In the case of ND compression, given the strong texture, extension twinning is not geometrically favored for most grains. Therefore, $\langle c+a\rangle$ pyramidal slip turns out to be the dominant fifth-independent slip system. In the case of 45° compression, part of extension twin variants become geometrically favored in many grains to act as the fifth deformation mode [26]. This is also evidenced by a considerable amount of extension twins in 45° compression sample (Fig. 2(c)). As a result, $\langle c+a\rangle$ pyramidal dislocations are inactive, as they require higher stress to multiply and glide.

Secondly, microstructural features, such as grain boundaries, dislocations, and precipitates, can reduce plastic anisotropy. In polycrystalline samples, a new term "effective CRSS" has been introduced to describe the stress values to activate each deformation mode [27]: $\tau^{eff.}=\tau^{true}+\Delta$, where τ^{eff} and τ^{true} are effective and true CRSS; Δ is the internal stress arising from grain boundaries, dislocations and particles. In the case of polycrystalline Mg, Hutchinson and Barnett reported that the ratio of the $\tau^{eff.}_{pris.}$ and $\tau^{eff.}_{basal}$ reduces as the dislocation density increases from deformation. We can apply their equation to pyramidal $\langle c+a\rangle$ and basal $\langle a\rangle$ dislocations:

$$\frac{\tau^{eff.}_{py}}{\tau^{eff.}_{basal}}=\frac{\tau^{true}_{py}+\alpha G b_{py}\rho^{1/2}}{\tau^{true}_{basal}+\alpha G b_{basal}\rho^{1/2}}$$

where τ^{eff}_{py} and τ^{eff}_{basal} are effective CRSS for $\langle c+a\rangle$ pyramidal slip and basal slip in polycrystals, respectively; τ^{true}_{py} and τ^{true}_{basal} are the true CRSS values in single crystal, respectively; α is a numerical constant; G is shear modulus; b_{py} and b_{basal} are Burgers vectors

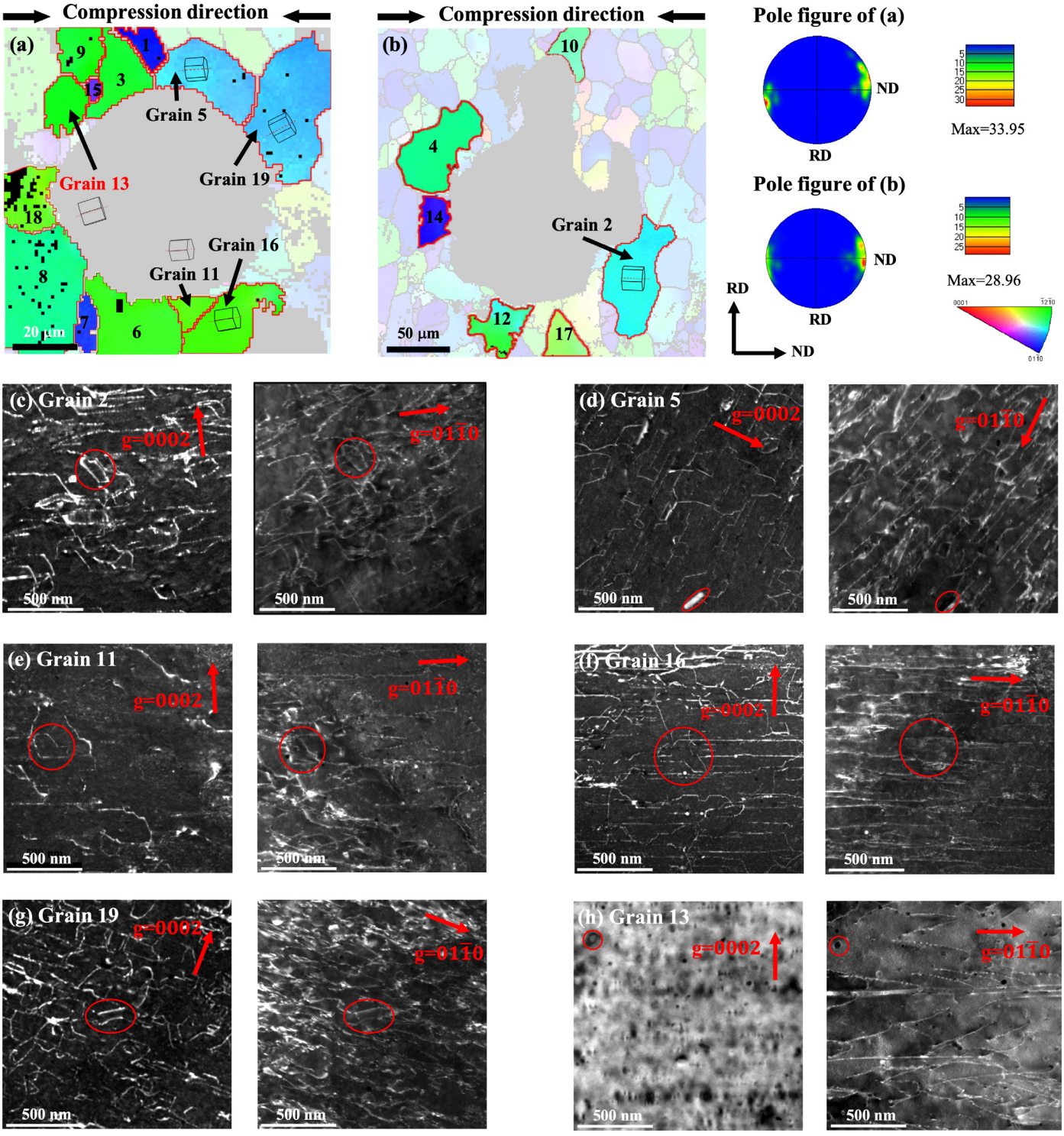

Fig. 3. (a) and (b) IPF maps of two specially designed TEM foils near the electropolished perforation region from the ND compression 2.6%-deformed AZ31 alloy. The schematic shows the orientations of labeled grains. The black arrows above each figure indicate the compression direction. (c)–(g) Examples of WBDF micrographs in 5 grains reveal their dislocation characters. The grain labels correspond to their locations in the foil in (a) and (b). Red circles are the fiducial markers to mark the identical sites. (h) BF and WBDF micrographs of Grain 13, showing the absence of $\langle c + a \rangle$ dislocations. (For interpretation of the references to color in this figure legend, the reader is referred to the web version of this article.)

for $\langle c + a \rangle$ and basal dislocations, respectively; ρ is dislocation density. Since b_{py} is larger than b_{basal}. The additive dislocation forest hardening term is greater for $\langle c + a \rangle$ dislocation, reducing the anisotropy effectively. The implication is that the pre-existing or early-emerging dislocations would make $\langle c + a \rangle$ pyramidal slip relatively easier in polycrystals. Applying this to the case of ND compression, grains with high *c-axis* off-angles may have basal dislocations at the very early stage, but those basal dislocations soon facilitate the ensuing $\langle c + a \rangle$ slip in the grain. This in part explains the profuse $\langle c + a \rangle$ dislocation activity in most grains of the ND samples, even in grains with large off-angle. For 45° compression sample, why $\langle c + a \rangle$ dislocations were not observed? This could

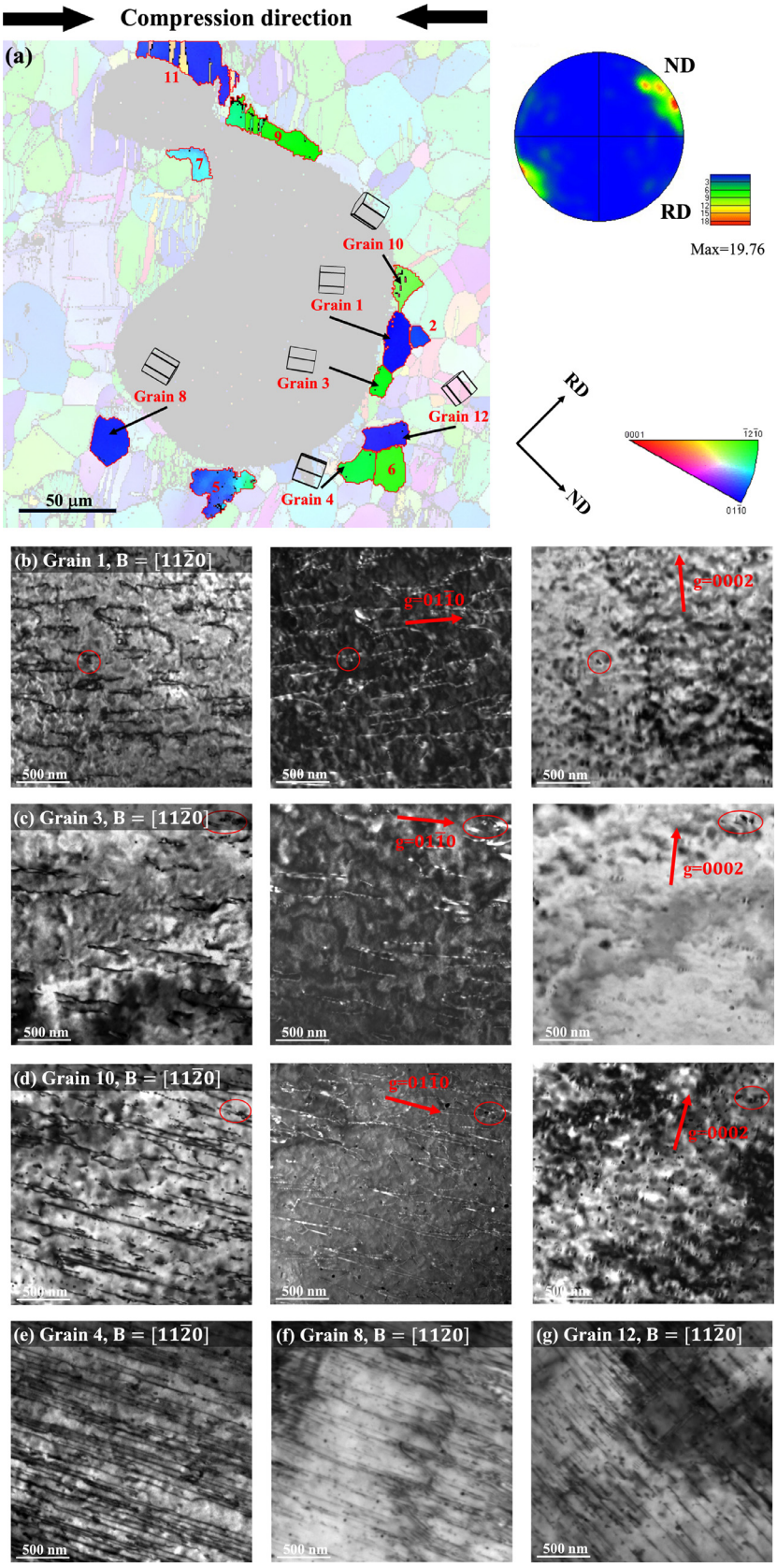

Fig. 4. (a) IPF maps of TEM foils near the electropolished perforation region from 45° compression 2.6%-deformed AZ31 alloy. The schematic shows the orientations of labeled grains. The black arrows above the figure indicate the compression direction. 12 grains are studied in total. Six representative grains are shown. (b)–(g) Examples of BF and WBDF micrographs in 6 grains reveal their dislocation activities. The grain labels correspond to their locations in the foil in (a). Red circles are the fiducial markers to mark the identical sites. (For interpretation of the references to color in this figure legend, the reader is referred to the web version of this article.)

be explained by the profuse {10–12} deformation twinning, which still requires lower stress than $\langle c + a \rangle$ slip at this strain level.

Lastly, the strain localization could be induced by {10–12} deformation twins, which leads to the suppression of $\langle c + a \rangle$ dislocations in the grains exhibiting small off-angles in the 45°-compression sample. Hazili et al. reported that the plastic deformation in polycrystalline Mg could be largely non-uniform when {10–12} extension twins are activated. Most plastic strain is mediated by twinning [28]. In our 45°-compression sample, the grains with large off-angles deform by dislocations along twinning and are "soft" grains; the grains with small off-angles deform by only dislocations and are "hard" grains. Up to the global strain of 2.6%, the "hard" grains experience much less strain than the "soft" grains. Thus, the local flow stress is not high enough to activate $\langle c + a \rangle$ slip in the "hard" grains.

In conclusion, $\langle c + a \rangle$ slip activities in grains of a highly textured polycrystalline AZ31 were statistically investigated using correlative microscopy. During ND compression up to 2.6% strain, $\langle c + a \rangle$ dislocations are active in most grains even for those with *c-axis* up to 30° off the compression axis. In contrast, in 45° compression, none of the examined grains has $\langle c + a \rangle$ slip activities even for those with *c-axis* merely 4° off the compression axis. The effect from the overall texture prevails over the orientation of individual grains in the deformation mode. It is a comprehensive result from the requirement of five independent slip systems and the reduction of anisotropy in polycrystalline Mg alloys. The former contributes to the activation and suppression of $\langle c + a \rangle$ dislocations in both ND and 45° compression samples. The latter explains the promoted activities of $\langle c + a \rangle$ slip in the ND sample. This direct observations and statistics of $\langle c + a \rangle$ dislocation activities in polycrystals could also serve as a benchmark for crystal plasticity modeling.

Declaration of Competing Interest

The authors declare that they have no known competing financial interests or personal relationships that could have appeared to influence the work reported in this paper.

Acknowledgments

The authors would like to acknowledge the funding support from the National Science Foundation (NSF-DMR, grant number: 1709865, program manager: Gary Shiflet) for the financial support for this research. The authors also would like to acknowledge the instrument and technical support from the Microscopy & Imaging Center and the Materials Characterization Facility at Texas A&M University.

Supplementary material

Supplementary material associated with this article can be found, in the online version, at doi:10.1016/j.scriptamat.2019.11.057.

References

[1] S.R. Agnew, Ö. Duygulu, Int. J. Plast. 21 (2005) 1161–1193.
[2] G. Proust, Science 365 (2019) 30–31.
[3] X.L. Ma, S. Eswarappa Prameela, P. Yi, M. Fernandez, N.M. Krywopusk, L.J. Kecskes, T. Sano, M.L. Falk, T.P. Weihs, Acta Mater. 172 (2019) 185–199.
[4] K.Y. Xie, Z. Alam, A. Caffee, K.J. Hemker, Scr. Mater. 112 (2016) 75–78.
[5] H. Yoshinaga, R. Horiuchi, Trans. JIM 5 (1964) 14–21.
[6] S.R. Agnew, J.A. Horton, M.H. Yoo, Metall. Mat. Trans. A 33 (2002) 851–858.
[7] J. Koike, Metall. Mat. Trans. A 36 (2005) 1689–1696.
[8] S. Sandlöbes, S. Zaefferer, I. Schestakow, S. Yi, R. Gonzalez-Martinez, Acta Mater. 59 (2011) 429–439.
[9] Z. Wu, W.A. Curtin, Nature 526 (2015) 62–67.
[10] Z. Wu, W.A. Curtin, Scr. Mater. 116 (2016) 104–107.
[11] Z. Wu, R. Ahmad, B. Yin, S. Sandlöbes, W.A. Curtin, Science 359 (2018) 447–452.
[12] T. Obara, H. Yoshinga, S. Morozumi, Acta Metall. 21 (1973) 845–853.
[13] J. Geng, M.F. Chisholm, R.K. Mishra, K.S. Kumar, Philos. Mag. Lett. 94 (2014) 377–386.
[14] J. Geng, M.F. Chisholm, R.K. Mishra, K.S. Kumar, Philos. Mag. 95 (2015) 3910–3932.
[15] B. Syed, J. Geng, R.K. Mishra, K.S. Kumar, Scr. Mater. 67 (2012) 700–703.
[16] E.W. Kelley, W.F. Hosford, Trans. Metall. Soc. 242 (1968) 5–13.
[17] E.W. Kelley, W.F. Hosford, Trans. Metall. Soc. 242 (1968) 654–661.
[18] B.-Y. Liu, F. Liu, N. Yang, X.-B. Zhai, L. Zhang, Y. Yang, B. Li, J. Li, E. Ma, J.-F. Nie, Z.-W. Shan, Science 365 (2019) 73–75.
[19] Y. Tang, J.A. El-Awady, Acta Mater. 71 (2014) 319–332.
[20] J. Zhang, S.P. Joshi, J. Mech. Phys. Solids 60 (2012) 945–972.
[21] J. Koike, T. Kobayashi, T. Mukai, H. Watanabe, M. Suzuki, K. Maruyama, K. Higashi, Acta Mater. 51 (2003) 2055–2065.
[22] V. Herrera-Solaz, J. LLorca, E. Dogan, I. Karaman, J. Segurado, Int. J. Plast. 57 (2014) 1–15.
[23] M.W. Vaughan, W. Nasim, E. Dogan, J.S. Herrington, G. Proust, A.A. Benzerga, I. Karaman, Acta Mater. 168 (2019) 448–472.
[24] K.Y. Xie, K.M. Reddy, L. Ma, A. Caffee, M. Chen, K.J. Hemker, Materialia (2019) 100504.
[25] D. Hull, D.J. Bacon, Introduction to Dislocations, 5th ed, Elsevier/Butterworth-Heinemann, Amsterdam, 2011.
[26] X.-L. Nan, H.-Y. Wang, L. Zhang, J.-B. Li, Q.-C. Jiang, Scr. Mater. 67 (2012) 443–446.
[27] W.B. Hutchinson, M.R. Barnett, Scr. Mater. 63 (2010) 737–740.
[28] K. Hazeli, J. Cuadra, P.A. Vanniamparambil, A. Kontsos, Scr. Mater. 68 (2013) 83–86.